

Results of the June 2000 NICMOS+NCS EMI Test

S. T. Holfeltz & Torsten Böker
September 28, 2000

ABSTRACT

We summarize the findings of the NICMOS+NCS EMI Tests conducted at Goddard Space Flight Center in June 2000. No NCS-induced noise was detected over a wide range of read-out sequences and compressor speeds. The sensitivity of the test data was close to on-orbit performance, thus the improved NCS design appears well suited for restoring NICMOS capabilities without degrading its sensitivity.

1. Introduction

The Near Infrared Camera and Multi-Object Spectrometer NICMOS is currently awaiting the installation of the NICMOS Cooling System (NCS). The NCS is a closed-loop, high-performance cooler that uses a high-speed compressor and turbines to circulate cryogenic Neon gas through the NICMOS dewar in order to cool the detectors to operating temperatures around 75 K.

Because of the high rotation speeds involved - the NCS turbines typically run at frequencies of a few kHz - and the rather high power consumption of the NCS, concerns were raised early in its development that the NCS could potentially cause electro-magnetic interference and/or conductance on the detectors of NICMOS or other HST instruments. Such unwelcome signals, commonly referred to as EMI/EMC, increase the effective read noise of the detectors and thus degrade their sensitivity.

Since NICMOS itself is inconveniently located in orbit, testing for EMI/EMC has to rely on the use of flight spare detectors in a dedicated dewar which is connected to the

NCS in a way that resembles as closely as possible the HST environment. The first EMI/EMC test was conducted in April of 1998 at Goddard Space Flight Center with support from the NICMOS IDT at the University of Arizona (Bergeron 1998, Schneider 1998). In that early test, operation of the NCS left an obvious signal in dark frames at frequencies between 5 and 9 kHz. Since this range corresponds to the range of NCS turbine frequencies, it was concluded that the NCS electro-mechanical design was not sufficiently shielded.

After a substantial re-design of the NCS Power Conversion Electronics (PCE), a similar test program was conducted in June 2000 to verify that the design changes were effective. Much effort was spent on improving the test conditions compared to the 1998 test. Pre-qualification tests compared two existing versions of the "Baseline Release Zero", or BRZ, detector read-out electronics to identify the one with minimal intrinsic noise. A number of different detector readout sequences were designed and implemented in the Science Instrument Test System (SITS) in order to be able to test for possible dependence on the detector clocking. In addition, the NCS telemetry was meticulously recorded to allow accurate off-line correlation with the detector data.

In a real team effort involving personnel from GSFC (logistics and ground system support), Creare Inc. (cooler hardware and operations), U of A (detector system maintenance and operations), and STScI (test sequence and scientific oversight), a second test was run from June 26-29 in the EMI clean room at GSFC, in order to shield the hardware from any environmental effects.

The NCS was connected electronically and mechanically in a flight-like manner to a liquid nitrogen dewar containing a NICMOS flight spare detector. Over the four days, about 1.2 GB of image and telemetry data was taken with the NCS running at various compressor speeds and with different detector readout sequences. The temperature of the detector was 77.30 ± 0.01 K for all data. The hardware setup and data formats for the June 2000 EMI test are described in Schneider (2000), as well as a detailed analysis of a subset of the test data. In this document, we describe the results of an independent analysis of all datasets in order to verify and generalize the Schneider (2000) conclusions.

This document is organized as follows. We describe the format of the test data in Section 2. The effective read noise levels and the test sensitivity are discussed in Section 3. In Section 4, we outline the data reduction procedure. Finally, the results of the power spectrum analysis are summarized in Section 5.

2. Test Data

Four different readout sequences were employed throughout the test program. These were designed to include both evenly and non-evenly spaced readouts as well as a variety of exposure times. The different readout sequences are outlined below and summarized in Table 1. Each of them was run both with the NCS off and operating at a number of different compressor speeds. The compressor speeds tested with each readout sequence are summarized in Table 2.

- **RN:** 30 two-read MULTIACCUM exposures with a 1.0 second integration time between the two reads (Δ -time). This sequence was used to establish the effective read-noise of the data.
- **UA:** 26 evenly spaced reads with Δ -time of 1.2 s. This sequence is identical to the one used in the 1998 test for direct comparison.
- **ST:** 10 reads with non-uniform Δ -times ranging from 0.3 to 7.0 seconds. This sequence was designed in order to be able to eliminate the possibility that any noise pattern was correlated with the detector clocks.
- **S2:** flight-like NSAMP = 18, SAMP_SEQ = STEP64 sequence with non-uniform Δ -times between 3.0 and 64.0 seconds for a total exposure time of 576 s per observation. This sequence was intended to provide an additional check under conditions that more closely resemble normal science operations than the first three sequences which were optimized for high data rates.

Table 1. Summary of readout sequences

Read #	Δ TIME			
	RN	UA	ST	S2
1	0.0	0.0	0.0	0.0
2	1.0	1.2	0.3	0.30
3		1.2	0.7	0.30
4		1.2	1.0	0.39
5		1.2	2.0	1.0
6		1.2	3.0	2.0
7		1.2	4.0	4.0
8		1.2	5.0	8.0
9		1.2	6.0	16.0
10		1.2	7.0	32.0
11		1.2		64.0
...	
18		1.2		64.0
19		1.2		
...		...		
26		1.2		

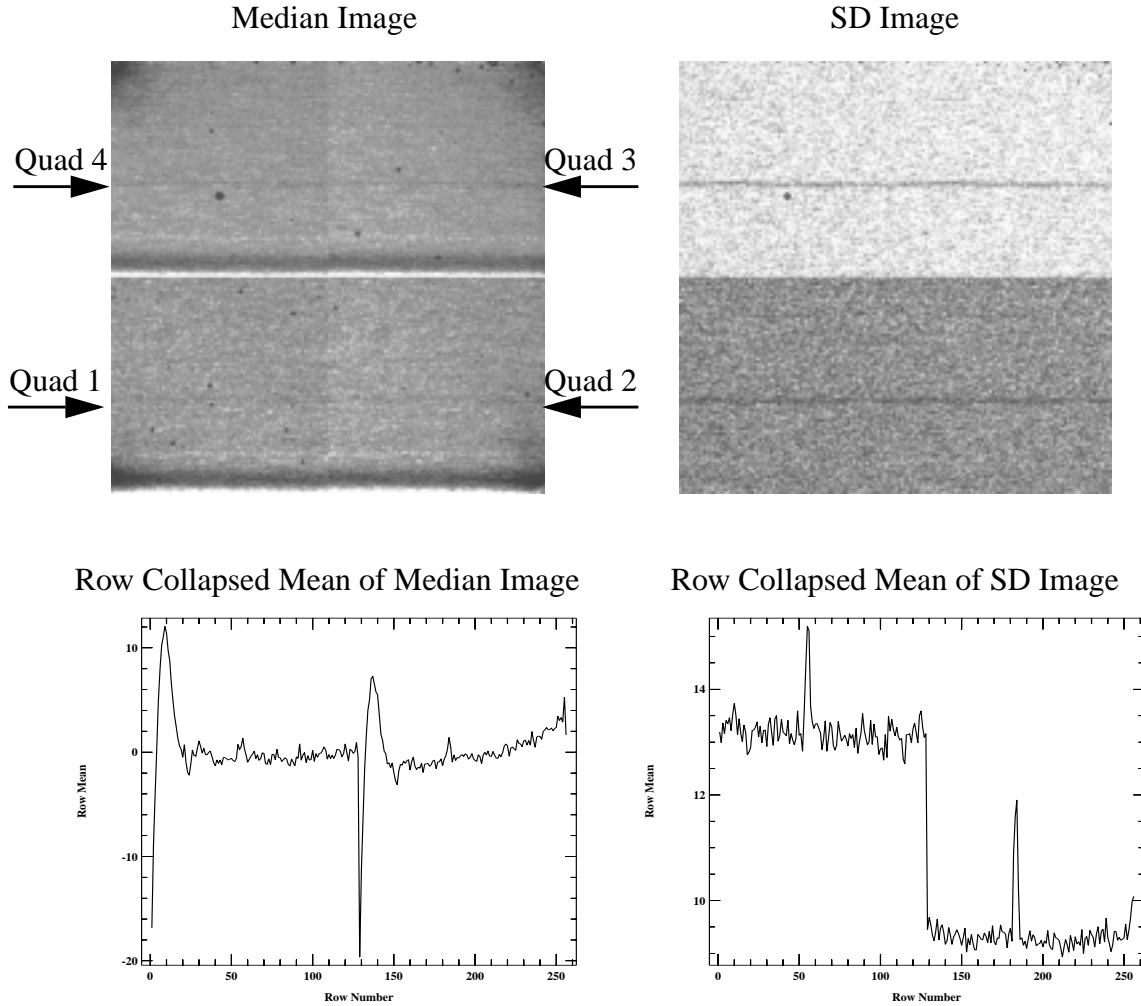
Table 2. Commanded compressor frequencies for each readout sequence

Readout Sequence	Commanded Compressor Frequency (Hz)
S2	6500, 7200
ST	5000, 5500, 5700, 5900, 6100, 6500, 6800, 7000, 7200
UA	5000, 5500, 5700, 5900, 6100, 6500, 6800, 7000, 7200

3. Sensitivity and Read Noise Estimate

Each of the 8 read noise datasets consists of 30 read pairs. Subtraction of the first from the second read of each pair removes the detector bias. The 30 difference images were median-combined (using the iraf task imcombine with 3-sigma clipping about the median). The resulting median image for one of the RN datasets is shown in Figure 1 (left panel).

Figure 1: Upper left: typical median image for a RN dataset. Upper right: image of the standard deviation. Higher counts are darker grey; the two images are not shown with the same stretch. The quadrant numbers are defined in the upper left panel. Plots of the row collapsed mean vs. row number for the median and standard deviation images are presented in the lower left and lower right panels, respectively.



Several characteristics of the read noise images are obvious in the above figure. The amplifier glow is evident in all four corners of the detector. The shading signal can clearly be seen in the first ~20 rows of each quadrant. Hot pixels appear as small dark spots. Quadrants 1 & 2 exhibit higher read noise than quadrants 3 & 4. There are faint bands of slightly elevated counts in most of the mean RN images; in Figure 1 they fall approximately at rows 56 & 182. These bands are repeatable, but not absolutely stable in location on the detector. They have a higher read noise as evident from Figure 1 and are most likely an artifact of the BRZ electronics (Schneider 2000). They are of no importance for the

noise analysis, and are described here only because they are apparent in some of the figures in this report.

The read noise per pixel is defined as the standard deviation about the median pixel value. In Figure 1 (right panel), we also show a typical distribution read noise per pixel. The average read noise per quadrant is reported in Table 3. As can be seen from the small spread of values, the read noise was fairly stable over the duration of the test. Averaged over all RN sequences, the mean read noise per pixel is 60.9 e⁻ for a two-read pair (assuming a gain of 5.4 e⁻/DN), which is about twice as high as the on-orbit NICMOS performance. However, since all four quadrants are read nearly simultaneously, they are susceptible to possible noise in an identical way. Their individual power spectra can therefore be averaged, which improves the overall sensitivity in identifying noise spikes by a factor of 2, close to on-orbit performance.

Table 3. Mean read noise per quadrant. The conversion from DN to electrons assumes a detector gain of 5.4.

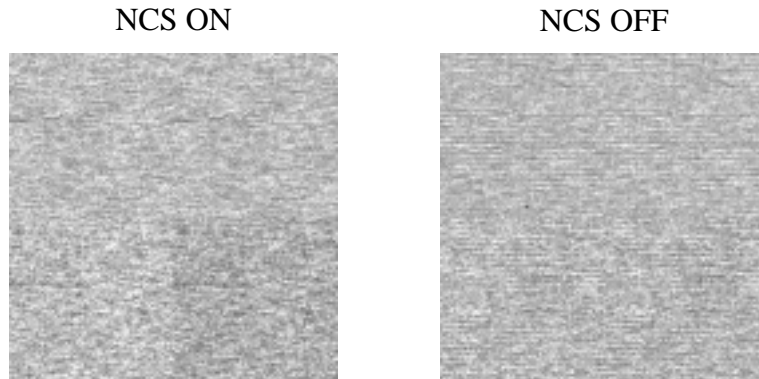
Dataset	Mean read noise per quadrant (DN)				Mean (e ⁻)
	1	2	3	4	
II00179124242	13.4	13.1	9.5	9.5	61.3
II00179174337	12.4	12.1	9.7	9.6	59.1
II00179220955	12.2	12.0	9.6	9.5	58.4
II00180124047	14.0	13.8	10.0	10.1	64.7
II00180151040	12.9	12.6	10.0	9.9	61.3
II00180180728	12.8	12.5	9.9	9.9	60.9
II00180183710	12.7	12.5	9.9	9.8	60.6
II00180220100	12.6	12.4	9.8	9.8	60.2
All RN Datasets	12.9	12.6	9.8	9.8	60.9

4. Data Reduction: Reference File Subtraction

In order to remove detector signatures such as dark current, amplifier glow, and bias from the test data, low-noise reference files were constructed in the following manner. For each day, *all* NCS-OFF datasets of a given readout sequence were median-combined, i.e. the nth read of the reference file was built from the median of the nth reads of all NCS-OFF files for that day and readout sequence. The appropriate reference file was then subtracted on a read-by-read basis from each data set of both NCS-ON and NCS-OFF sequences. Figure 2 provides examples of calibrated (reference-subtracted, zeroth read

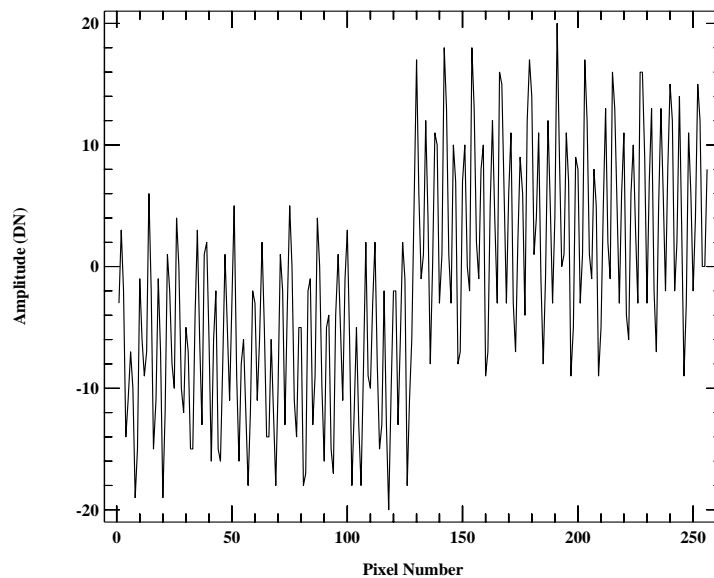
subtracted) frames from the ST sequence. The 60 Hz and 180 Hz signal (see Section 5 below) is readily apparent.

Figure 2: Examples of reference-subtracted, zeroth read subtracted data frames from the ST sequence. The greyscale stretch is the same for both images, higher counts are darker grey.



A plot of the row median vs. row number (for extension 1 of the dark subtracted NCS-ON ST dataset) is presented in Figure 3. In addition to the bias difference of individual quadrants, the figure shows that the amplitude of the 60 Hz signal in the calibrated images is approximately 10 DNs.

Figure 3: Row Median vs. Row Number Showing Signal Amplitude



5. Fourier Analysis

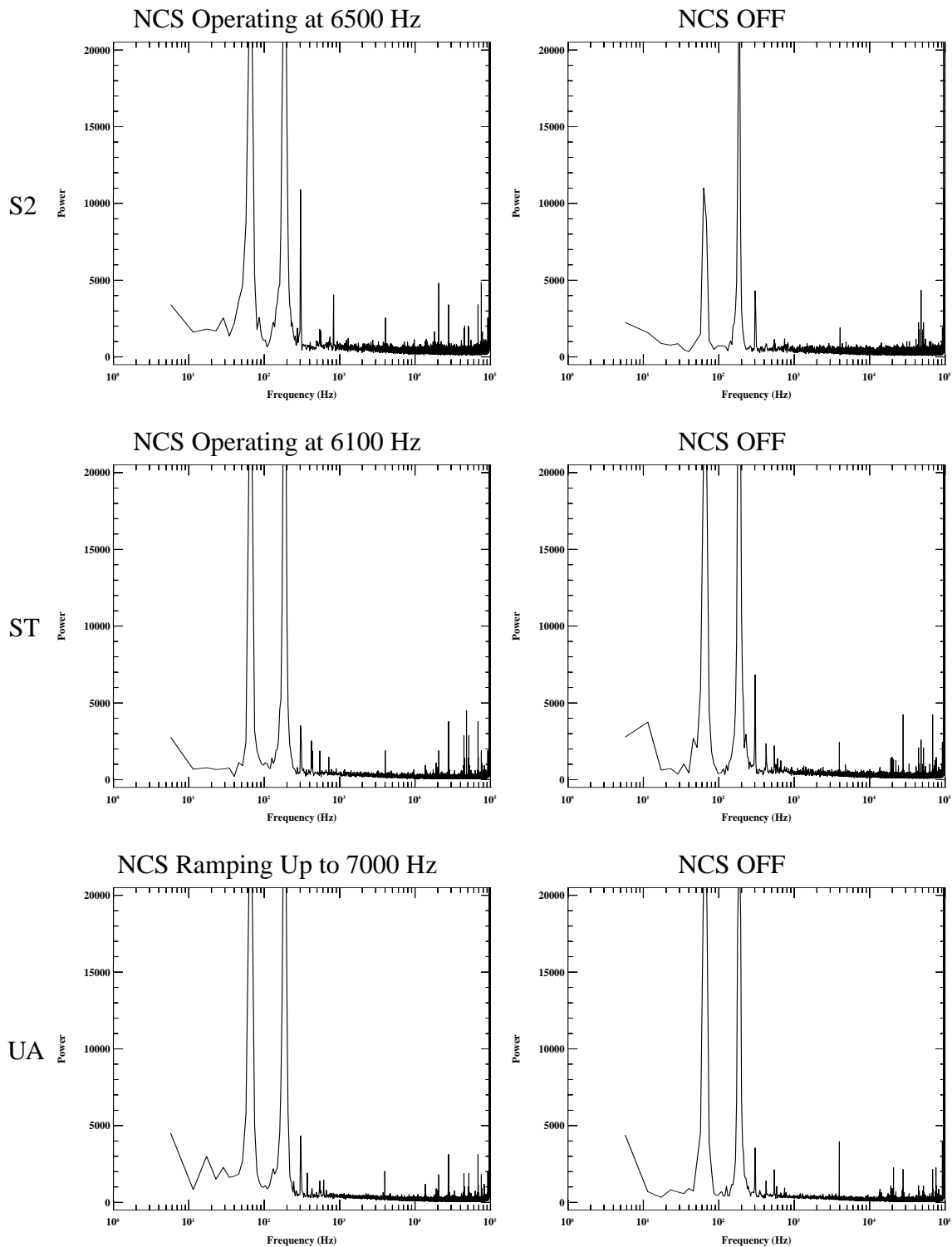
In order to identify and analyze possible noise components introduced by the operation of the NCS, we calculated power spectra of each quadrant independently for all reads of a given dataset. Because the data are overclocked by 21 μ seconds (2 cycles of the horizontal pixel clock of 10.5 μ seconds), two additional columns of data were introduced at the end of each row. This simulates data taken at evenly spaced intervals in time and thus allows the use of standard Fast Fourier Transform (FFT) routines. The power spectra of all reads were then averaged to increase their signal-to-noise ratio. Averaging the power spectra of the four quadrants further increases the sensitivity to imprinted signals by a factor of 2. Figure 4 shows the mean power spectra for six example datasets¹.

The strong signal components at 60 Hz and 180 Hz are present in all datasets (albeit with a somewhat varying relative power), irrespective of whether the NCS was running or not. They, as well as some other small signals at higher multiples of 60 Hz are undoubtedly caused by variations in the voltage supply, and should be ignored for the purpose of this analysis. The important conclusion that can be drawn from Figure 4 is that **operation of the NCS did not produce any noticeable signal in the power spectra**, i.e. the NCS-ON data are indistinguishable from the NCS-OFF data. This is true even for datasets taken during ramp-up or shutdown of the NCS (upper left panel in Figure 4). Although we only show the results for six datasets, we point out that the power spectra from *all* observations were visually inspected and were found to be consistent with those presented here.

The analysis outlined above was carried out separately on individual reads, first difference frames, and zeroth read subtracted frames. No substantial differences were found, indicating that the detector reset level is also free from any NCS-induced signal.

1. One NCS-ON and one NCS-OFF dataset from each of the three readout sequences were chosen as examples. The examples were chosen to include both days 179 and 180 as well as a variety of NCS compressor speeds, including one dataset taken while the NCS was ramping up. The datasets chosen were as follows. S2: I00179215056_2RUV4A2 with the NCS at 6500 Hz and I00179210356_2RUV4A3 with the NCS off; ST: I00180135531_2RUV4AG with the NCS operating at 6100 Hz and I00180125409_2RUV4A7 with the NCS off; and finally, UA: I00180125726_2RUV4AC during which the NCS was ramping up to 7200 Hz and I00180124904_2RUV4A1 for which the NCS was off.

Figure 4: Mean power spectra for some example datasets. The low power, monochromatic peaks at higher frequencies are repeatable but intermittent.



6. Conclusions

Our analysis has confirmed the results reported by Schneider (2000) that no NCS-imprinted EMI/EMC signal was found in the test data. Since other instruments on board HST will not be coupled as closely to the NCS as NICMOS, installation and operation of the NCS onboard HST is unlikely to degrade the read-noise performance of NICMOS or any other HST instrument.

7. References

- Schneider, G. 2000, "Results From the NCC/NICMOS Spare-Detector June 2000 EMI Test", report to NASA/GSFC and STScI
- Bergeron, L. E 1998, "NICMOS/NCS EMI Test Data Results", NICMOS TIR 98-001.
- Schneider, G. 1998, "EMI Noise Properties of the NICMOS Cooling System as Seen by a NICMOS-3 Flight Spare Detector", report to NASA/GSFC and STScI